ELSEVIER

Materials Science and Engineering A238 (1997) 50–65

MATERIALS SCIENCE & ENGINEERING A

# Influence of residual stresses on the evolution of microstructure during the partial reduction of $NiAl_2O_4$

E. Üstündag [a,*], Z. Zhang [c], M.L. Stocker [c], P. Rangaswamy [b], M.A.M. Bourke [b], S. Subramanian [c], K.E. Sickafus [a], J.A. Roberts [b], S.L. Sass [c]

[a] *Materials Science and Technology Division, Los Alamos National Laboratory, Los Alamos, NM 87545, USA*
[b] *Manuel Lujan Jr. Neutron Scattering Center, Los Alamos National Laboratory, Los Alamos, NM 87545, USA*
[c] *Department of Materials Science and Engineering, Cornell University, Ithaca, NY 14853, USA*

**Abstract**

Metal-ceramic microstructures were formed in situ by the partial reduction (i.e. the reduction of only one of the metallic elements) of the spinel compound $NiAl_2O_4$. Depending on reduction conditions, these microstructures consist of Ni particles embedded in an $\alpha$-$Al_2O_3$ or a multiphase matrix called 'defect spinel'. The volume shrinkage that accompanies the reaction generates residual stresses which profoundly affect the microstructure evolution. Conversely, formation of metastable, intermediate phases, generation of porosity and cracking are all observed and may act to relax the residual stresses. Electron microscopy observations as well as both neutron and X-ray diffraction residual stress measurements are used to study the influence of residual stresses on the microstructure evolution during the reduction process. © 1997 Elsevier Science S.A.

*Keywords:* Residual stresses; Microstructure; $NiAl_2O_4$; Reduction reactions

## 1. Introduction

Ceramics by virtue of their chemical inertness and typically high compressive strengths are attractive candidates for structural applications at high temperatures in high stress and corrosive environments. Unfortunately, because of their low fracture toughness it is mostly not possible to use them in their monolithic form. One strategy for circumventing their low toughness is to incorporate them into a ceramic composite, where the second component improves fracture resistance. In situ processing techniques are currently being studied for the fabrication of such composites in a cost-effective manner.

One such approach involves the partial reduction of either oxide compounds or solid solutions which contain at least two cations, one more reducible than the other [1]. Metal-ceramic microstructures can be formed from the spinel compound, $NiAl_2O_4$, which in the presence of a reducing atmosphere undergoes partial reduction according to the equation,

$$NiAl_2O_4 \Rightarrow Ni + \alpha\text{-}Al_2O_3 + 1/2O_2. \quad (1)$$

Elrefaie and Smeltzer [2] studied the phase equilibria for this reaction. Since oxygen is being removed there is an associated volume decrease, which, based on the molecular weights and crystallographic densities of the phases involved, is calculated to be $\sim 17.6\%$. As we shall report, experimental measurements give actual volume decreases of between 3 and 9%, which demonstrates that the system finds a mechanism to avoid generating such large volume changes and in so doing relaxes the stresses associated with the reduction reaction. Nevertheless, even for these smaller volume changes, large stresses can still be generated.

For the spherical geometry illustrated in Fig. 1, the reduction reaction is expected to proceed from the outside surface inward. Due to the volume shrinkage during reduction, the outer layer, consisting of a two phase mixture of Ni + '$Al_2O_3$', should exhibit a tensile hoop stress, provided that it does not crack. The alumina is shown in quotes here because, as will be discussed later, the stable room temperature form $\alpha$-$Al_2O_3$ is not always obtained and metastable phases, such as $\theta$-$Al_2O_3$, are found under some reduction conditions.

* Corresponding author. Present address: Department of Materials Science, Mail Code 138-78, California Institute of Technology, Pasadena, CA 91125, USA.


*PII* S0921-5093(97)00433-4

An elasticity calculation was performed for this spherical geometry assuming no relaxation of stresses by creep or plastic deformation. Using the small strain approximation we assumed a volume change ($\Delta V/V_i$) of $-5\%$. For a specimen in which the transformed layer has a thickness half that of the sphere radius, the calculation predicted a tensile hoop stress of $+1.7$ GPa at the interface and $+0.52$ GPa at the surface, while the internal hydrostatic pressure in the spinel phase was $-2.4$ GPa. Other details of the calculation are presented elsewhere [3].

It is likely that a considerable portion of these stresses will be relaxed by plastic/creep deformation and diffusional processes at high (i.e. reduction) temperatures. The collapse (or sintering) of pores in the unreduced spinel when it is under compression is one example for these processes. If that occurs, then an in situ hot isostatic pressing is realized, with a decrease in the amount of porosity expected after reduction.

Cracking of the reduced layer is another probable stress relaxation mechanism. During the early stages of this study cracking was a recurrent problem, but was precluded by incorporating 2.5–10 wt.% $ZrO_2$ to the initial spinel powder before hot pressing [4]. $ZrO_2$ suppressed cracking during reduction by inhibiting grain growth in the initial spinel [4]. Since cracking was primarily observed along the original spinel grain boundaries, a finer grain size leads to an increase in grain boundary area and hence, to a higher energy requirement for cracking to occur. It was also noted that a critical grain size exists for pure spinel ($\sim 15$ μm diameter) beyond which cracking is encountered again [5]. This observation of a critical grain size is considered strong evidence that elastic energy is being stored within the grains as a result of the reduction reaction. Based on this observation a simple calculation was made of the elastic strain, where at the critical grain radius, the stored elastic energy that is released is sufficient to produce the new surfaces of the cracked grain boundaries [6]. This showed that residual stresses of several hundred MPa can be generated and supported during reduction before grain boundary cracking occurs. All of these observations point to the existence of residual stresses generated by the volume shrinkage during reduction.

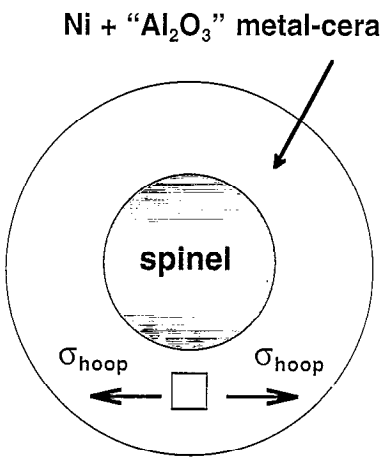


Fig. 1. Schematic diagram of a partially reduced spherical specimen, where the inner untransformed spinel is surrounded by a spherical shell of the reduced two phase mixture of Ni + '$Al_2O_3$'.

The two natural questions that follow are: (1) What is the effect of these stresses on the microstructure of the reduction product? (2) How much relaxation takes place during the reaction? The second question is addressed in another publication (unpublished) that describes our attempts to utilize the residual stresses that can be generated by this reduction reaction to place outer surfaces of ceramics under compression so that their fracture resistance is enhanced (i.e. 'tempering'). The present paper concentrates on the first question and presents our observations about the effect of residual stresses on microstructure evolution.

First, microstructures obtained at different stages of the reduction will be presented. Then scanning electron microscopy observations and density measurements will be used to examine the possibility of the in situ hot isostatic pressing of spinel during reduction. Mechanical testing results will be utilized to examine the Young's modulus of the reduced composite in relation to its microstructure. Finally, X-ray and neutron diffraction residual stress measurement data will be presented that demonstrate the generation of stresses by the volume decrease.

## 2. Experimental procedure

### 2.1. Sample preparation

Polycrystalline $NiAl_2O_4$ samples (with or without $ZrO_2$) were prepared by hot pressing in alumina dies using a uniaxial hot press for 2–4 h at 1600°C in air, with 23–30 MPa pressure. All work in this study used $NiAl_2O_4$ powders of less than 4 μm grain diameter. The resulting density of all hot-pressed samples was better than 90% of the theoretical density. The hot-pressed samples were partially reduced at oxygen activities below the stability limit of the spinel (as specified in [2]) using $CO/CO_2/N_2$ gas mixtures and at temperatures between 1100 and 1400°C. Other details of sample preparation are presented elsewhere [1,4].

### 2.2. Specimen polishing

Proper polishing of samples is critical for scanning electron microscopy (SEM) studies of microstructure. The main technique employed in this work consisted of mechanical polishing, however, different versions of

this technique were developed and adapted depending on the material and the analysis method for which it was required.

Initially the most common polishing technique involved using SiC papers with grit sizes of 120–1200, successively, on a rotating wet-polisher to flatten and level the specimens. A finer polishing was accomplished by using 6, 3 and 1 μm diamond paste, successively, with an oil-based extender on a long-hair Ceripol™ cloth (South Bay Technology, San Clemente, CA). However, due to the extensive grain and particle pull-out observed in both unreduced spinel and reduced composite samples, this method was discontinued and a systematic study was made to develop the best polishing technique. For both types of samples, the initial SiC paper sequence on a wet-rotary polisher followed by a 1 μm SiC paper, again on a wet-polisher, yielded the least amount of pull-out as well as the minimum rounding of specimen edges.

Specimens were polished more efficiently and uniformly when mounted on polishing cylinders (38.1 mm diameter, 25.4 mm high) which were placed inside cylindrical rings with one end well machined to give a surface perpendicular to the axis of the ring and which also fit tightly around the cylinder. This configuration allowed for an equally distributed pressure to be applied during polishing and minimized the wobble of the sample.

### 2.3. Electron microscopy

SEM studies were carried out using backscattered and secondary electron imaging in a JEOL 733 electron microprobe and a Leica 440 Stereoscan microscope. Transmission electron microscopy (TEM) was carreid out on a JEOL 1200 EX and a Philips CM 30 by bright field imaging and electron diffraction. Scanning transmission analytical microscopy (on JEOL 200 CX, VG501 and VG HB601UX) techniques were used to examine the microstructures, and to determine the phases present and their compositions.

Energy-filtered imaging in a scanning transmission electron microscope, a STEM (VG 501), provided a thickness map of the specimen and probed the pores in the $Al_2O_3$ for gaseous oxygen content. Energy filtered images were recorded at the bulk plasmon energy of 26 and at 8 eV where the low loss spectrum of $O_2$ exhibits a distinctive feature absent in the low loss spectrum on $Al_2O_3$ [7]. The ratio of the energy filtered image recorded at 26 eV to the bright field image was used to obtain a thickness map of the specimen [8].

Another VG STEM (HB601UX) operating at 100 kV was employed to obtain the chemical composition of the phases present around the reduction front using a Oxford Instruments-Link energy-dispersive X-ray spectrometer (EDXS).

### 2.4. Density, volume change and weight loss measurements

Density measurements were carried out using the boiling water method (ASTM Standard C 373-88) [9] which utilizes Archimedes' principle to determine bulk density, open porosity, water absorption and apparent specific gravity and indirectly, closed porosity. The procedure involves immersing specimens in boiling water for 5 h after which they are allowed to soak for an additional 24 h. During the boiling period water vapor is assumed to penetrate all the accessible surface-connected (open) pores and upon its condensation during cooling, the pressure difference generated drives liquid water into these pores. Internal checks were performed on the validity of the procedure and a commercial alumina (Coors AD-998E, Coors Ceramics Company, Golden, CO) with known density was tested to check the accuracy of the method. It was determined to be quite accurate, yielding experimental errors of less than 10%. The entire procedure was performed several times on the same samples before and after reduction to check reproducibility.

Volume changes were determined experimentally by measuring initial and final dimensions using either a digital or a mechanical Mitutoyo micrometer capable of 1 μm resolution. Both the density and volume change measurements were performed on cylindrical pellets (10–13 mm in diameter and 2–5 mm thick). Volume change measurements were also checked using the initial and final values of the external volume of specimens obtained during the density measurements by the boiling water method. Volume change results from the two techniques were in reasonable agreement differing by less than 25% from one another.

Due to the release of oxygen during reduction, there should be a decrease in weight after the reaction, which is calculated to be 9.1% using the molecular weights of the phases involved [10]. To determine whether all the excess oxygen is released to the environment, samples were carefully weighed before and after reduction with 0.0001 g resolution. They were heated for several hours at 100–125°C to remove entrapped moisture before reduction and weighed immediately after reduction while they were still hot.

### 2.5. Mechanical property characterization

To investigate the effect of processing parameters on the mechanical properties of the reduced metal-ceramic composite its elastic constants were determined at room temperature using the pulse-echo ultrasonic technique (see for example, [11]).

### 2.6. X-ray and neutron diffraction techniques

Residual stresses in specimens were determined at the Manuel Lujan Jr. Neutron Scattering Center (MLNSC) at Los Alamos using X-rays and neutrons. The X-ray diffraction (XRD) was carried out with Cu K$\alpha$ radiation which has a shallow penetration depth ( $\leq 20$ μm) in alumina. Therefore, the irradiated region was assumed to be under plane stress conditions and the classical '$d$ versus $\sin^2\psi$' approach [12] was used employing the (416) peak of $\alpha$-$Al_2O_3$ ($2\theta \approx 136°$). Stress measurements were made by collimating the X-ray beam to obtain a spot size of 1 and 3 mm on the specimens. The X-ray elastic constants used were calculated from bulk values ($E = 340$ GPa, $\nu = 0.22$) of $\alpha$-$Al_2O_3$ (Alsint 99.7—Bolt Technical Ceramics, Conroe, TX).

In contrast with X-rays whose penetration is limited to surfaces, neutrons can penetrate several tens of millimeters into most materials. The low attenuation enables many grains to be examined, giving a representative value of the internal strains in grains of particular orientations. Elastic strains are determined from changes in lattice spacings from a 'stress-free' value [13]. At spallation neutron sources (such as the one at Los Alamos) pulses of neutrons are used. The wavelength of a detected neutron is determined from its time of flight between creation by the spallation process and arrival at the detector. Thus the specimen is scanned very rapidly in wavelength and after many pulses gives a spectrum containing all the lattice spacings. Determination of all the lattice spacings gives a comprehensive measurement of the microstructural stress state [13]. The specific spectrometer used in this study was the neutron powder diffractometer (NPD) at MLNSC.

## 3. Results

### 3.1. Microstructure observations

In order to better understand the evolution of microstructure during the reduction of $NiAl_2O_4$ we first present some electron microscopy observations. Fig. 2 shows a TEM bright field image of the microstructure at the reduction front in a specimen reduced at 1100°C. It is seen that crystallographically oriented Ni particles form in a matrix identified as 'defect spinel' [1]. It was shown earlier that there is a fcc twin orientation relationship (a (111){112} twin) between the Ni and the matrix suggesting an attempt by the system to lower strain energy [1]. Fig. 2 also reveals some microcracking, though on a much smaller scale than observed earlier [4].

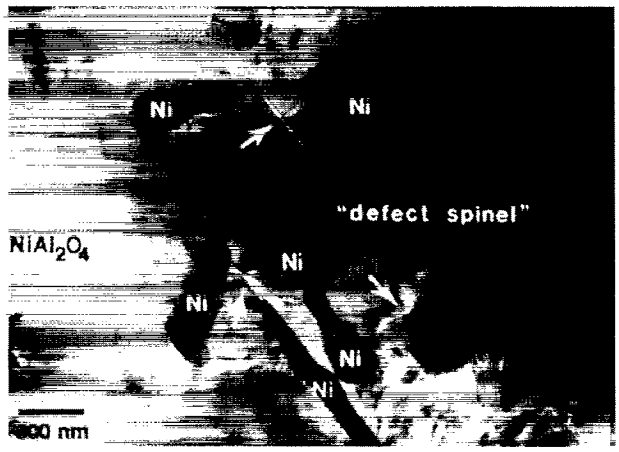


Fig. 2. Transmission electron micrograph of the reduction front in a specimen reduced at 1100°C for 4 h at an oxygen activity of $10^{-14}$. The arrows indicate microcracks developing during reduction.

The major phase in 'defect spinel' appears to be $\theta$-$Al_2O_3$ (Fig. 3). There are also additional unidentified peaks which point to the presence of other phases (see [16] for details). Phases such as $NiAl_6O_{10}$ and $NiAl_{10}O_{16}$ have been observed in previous studies on the Ni-Al-O system [18]. $\theta$-$Al_2O_3$, though monoclinic, has a nearly cubic oxygen sublattice [14,16]. This metastable form of alumina has also been detected in other reactions where a cubic oxygen sublattice (in $\gamma$-$Al_2O_3$) is transformed into a hexagonal one (in $\alpha$-$Al_2O_3$) [15,17]. In this case, it was seen that the $\theta$-$Al_2O_3$ to $\alpha$-$Al_2O_3$ transformation is kinetics-controlled and given enough time, it reaches completion. The theoretical volume change during this transformation is $-10.2\%$ (calculated using the theoretical densities of each alumina phase: 3.62 g cm$^{-3}$ for $\theta$-$Al_2O_3$, 3.99 g cm$^{-3}$ for $\alpha$-$Al_2O_3$). Wilson and Stacey [17] observed a change in the morphology of the porosity (reduction in the number of pores and enlargement of their average size) present in their samples (this porosity was remnant from the beginning of the reaction when boehmite transformed to $\gamma$-$Al_2O_3$). They also mentioned a shrinkage in sample volume but did not give a value.

Our observations are in accordance with Wilson and Stacey. We also see that the $\theta$-$Al_2O_3$ to $\alpha$-$Al_2O_3$ transformation is a kinetically-favored step, since the latter alumina phase starts forming in samples held for more than 144 h at 1100°C [19].

Fig. 4 is a view of the reduction front in a sample reduced at 1300°C. It is interesting to note the presence of 'defect spinel' at such a high temperature. In fact, 'defect spinel' is found at reduction fronts in specimens reduced even at 1400°C [15]. The presence of 'defect spinel' at any reduction temperature clearly proves that it forms as an intermediate step during the transformation of $NiAl_2O_4$ to Ni + $\alpha$-$Al_2O_3$.

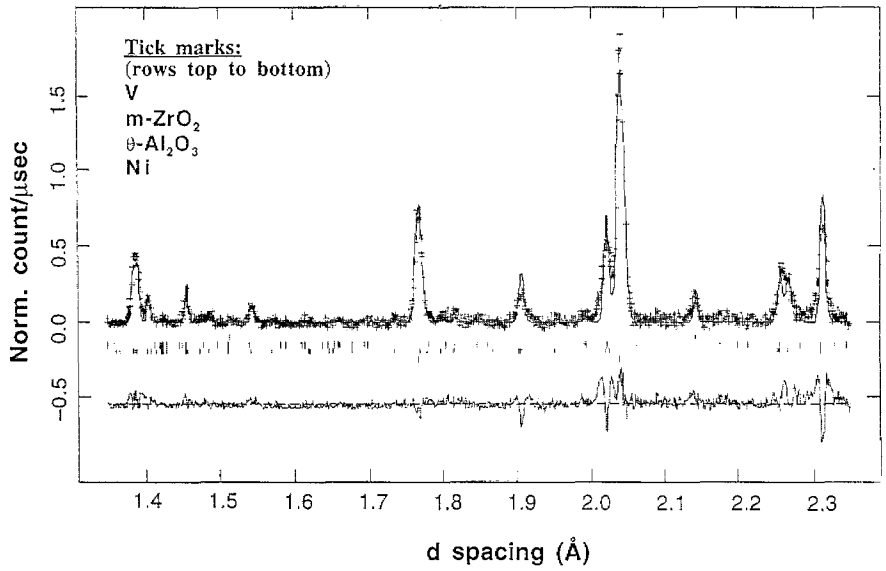


Fig. 3. Part of the neutron powder diffraction pattern obtained from a specimen reduced at 1100°C for 24 h in an approximate oxygen activity of $10^{-16}$. The raw data is designated with 'crosses'. The solid line that is fitted to this data was obtained by performing Rietveld analysis. The four phases present in the pattern are shown in the figure. The sample was doped with 10 wt.%$ZrO_2$ to avoid cracking during reduction, and almost all of this phase was determined to be monoclinic. The V (vanadium) comes from the holder plate used to position the specimen in the diffractometer. The lower curve in the figure designates the difference between the raw data and the Rietveld fit to it. The $\theta$-$Al_2O_3$ was determined to be monoclinic with a space group of A 2/m and lattice constants of $a = 5.615$, $b = 2.909$ and $c = 11.787$ Å and $\beta = 104.078°$ (values similar to the crystallographic data in the literature [14]).

A chemical analysis across the reduction front in Fig. 4 (indicated by a line) has been performed using a STEM (Fig. 5). The unreduced spinel was found to have 10–13 at.% Ni. When the reduction front is crossed, the Ni concentration drops to about 4 at.%. This shows that the 'defect spinel' is Ni-poor. Furthermore, it appears to be multiphase since the region between Ni particles 1 and 3 in Fig. 4 shows a different Ni concentration (4–8 at.%) than that found in the first region. The first Ni particle is nearly pure; with the small amounts of Al and O found in it probably resulting from an underlying layer of oxide. It should also be noted that the orientation of this particle with respect to the X-ray detector in the STEM was not edge-on leading to an interface between the particle and the matrix which is inclined to the electron beam. To summarize, the STEM data indicate that at the reduction front the Ni phase starts precipitating soon after the formation of a Ni-poor, multiphase 'defect spinel' matrix. Further STEM investigations are planned to examine how 'defect spinel' transforms to the equilibrium matrix phase of $\alpha$-$Al_2O_3$.

Fig. 6 shows a typical region in the same sample further away from the reduction front where the matrix is still 'defect spinel'. The width of this region is about 20 μm in this sample. The Ni particles in this region are mostly along the original spinel grain boundaries and usually crystallographically oriented. Porosity is also observed, mostly at grain boundaries. In specimens doped with $TiO_2$ and reduced under the same conditions the width of this region can be as narrow as 50–100 nm [19].

The equilibrium microstructure for this sample is shown in Fig. 7 where irregularly-shaped Ni particles and pores are observed together with an $\alpha$-$Al_2O_3$ matrix. In addition to the large Ni particles (1–4 μm in diameter) along the $\alpha$-$Al_2O_3$ grain boundaries there are much smaller ones (20–250 nm in diameter) inside the grains. The Ni particle size therefore shows a bimodal distribution.

The microstructural observations so far can be summarized as follows: The reduction of $NiAl_2O_4$ involves an intermediate step where a multiphase matrix called 'defect spinel' forms before the equilibrium $\alpha$-$Al_2O_3$ matrix is obtained at all reduction temperatures studied. At 1100°C reduction, the $\alpha$-$Al_2O_3$ stage is never reached for times less than 144 h. During this period the major 'defect spinel' phase is the metastable, monoclinic $\theta$-$Al_2O_3$. The microstructure consists of crystallographically oriented Ni particles with some residual Ni found in the matrix in the form of other metastable phases. At 1300°C, the reduction for short times (several hours or less) does, however, yield the $\alpha$-$Al_2O_3$ matrix. The low temperature Ni + 'defect spinel' microstructure is still found at this temperature as an intermediate layer between the unreduced spinel and the equilibrium microstructure. An important microstructural parameter for all reduction conditions appears to be the presence of porosity in the matrix. Several studies were performed to obtain quantitative

information on porosity and to investigate the possibility of in situ hot isostatic pressing, with the results outlined in the next two sections.

### 3.2. Scanning electron microscopy observations

The first method to determine the amount of porosity used the digital imaging capability of a scanning electron microscope (JEOL 733). It was assumed that the area fraction of a structural feature (porosity in this case) is equal to its volume fraction. It should also be understood that the measurements by this technique are highly sensitive to the contrast and brightness in the images. To check this, different images of the same region were processed under varying imaging conditions and it was determined that the sensitivity was $\pm 1$ vol.%. Furthermore, the porosity values obtained by this technique were compared to those obtained by the ASTM density measurement method described in the following section and the values were similar to within a few vol.% for the unreduced specimens.

Initial efforts to observe the change in porosity during reduction were unsuccessful due to the improper polishing method employed. It was shown that extensive grain pull-out occurred in unreduced spinel, which in turn yielded a much higher initial porosity than actually present before reduction. Fig. 8 (a,b) illustrates the extent of grain pull-out that occurs due to incorrect polishing (the dark regions are pores, the gray is spinel and the bright particles are $ZrO_2$). The sample in Fig. 8 (a) has 11–12 vol.% porosity, whereas the one in Fig. 8 (b) has only 1–1.5 vol.%. Both micrographs were taken on the same sample with the only difference being the polishing technique. It is seen that an extensive amount of damage can be introduced during the mechanical polishing of a brittle ceramic such as spinel.


Fig. 4. Transmission electron micrograph of the reduction front in a pure spinel specimen reduced at 1300°C for 2 h at an oxygen activity of $10^{-12}$. There are four Ni particles visible (dark) and are numbered. The line drawn is the position of the line trace performed on STEM to determine the variation of chemical composition across the reduction front as illustrated in Fig. 5.

After the polishing artifacts were minimized, a more reliable comparison was possible between the unreduced and reduced specimens. Fig. 9 (a,b) shows SEM micrographs of the same sample before and after reduction, respectively. The total porosity measured in the unreduced sample was between 9 and 12 vol.%, while the reduced sample showed less than 2 vol.% porosity (the bright regions in Fig. 9 (b) are mostly Ni particles plus some $ZrO_2$ while the matrix is $\alpha$-$Al_2O_3$). Similar results were seen in samples with different amounts of initial porosity. This indicates that flaw healing in the form of a decrease in the amount of porosity may be occurring during reduction probably due to the in situ hot isostatic pressing of the unreduced portion of spinel. Another possibility exists, however, where the pore size may have decreased to a dimension small enough to prevent observation by SEM. This behavior may have also been accompanied by smearing (or plastic deformation) of Ni metal particles that would fill the nearby pores and lead to an apparently smaller amount of porosity on the SEM. A decrease in the size of the pores, if that is happening, would indicate the occurrence of flaw transformation instead of flaw healing. To clarify this issue a more accurate method of determining the final porosity in reduced samples was needed and the ASTM standard density measurements described in the next section provided that capability.

### 3.3. Density, volume change and weight loss measurements

#### 3.3.1. Density measurements

*3.3.1.1. Specimens reduced at 1300°C.* The results for unreduced samples and those reduced at 1300°C for 6 and 24 h at an oxygen activity of $a_{O_2} = 10^{-12}$ (using a mixture of 96% CO + 4% $CO_2$ diluted in 90% $N_2$) are presented in Table 1 (samples are sorted with respect to initial, i.e. before-reduction, total porosity). All samples shown in Table 1 consisted of Ni + $\alpha$-$Al_2O_3$ after reduction with no remnant 'defect spinel' in the matrix. Fig. 10 plots the sample number versus final, i.e. after-reduction, total porosity together with the corresponding volume change data (discussed in Section 3.3.2). The measurements were repeated several times on selected samples to check the reproducibility. In all cases the

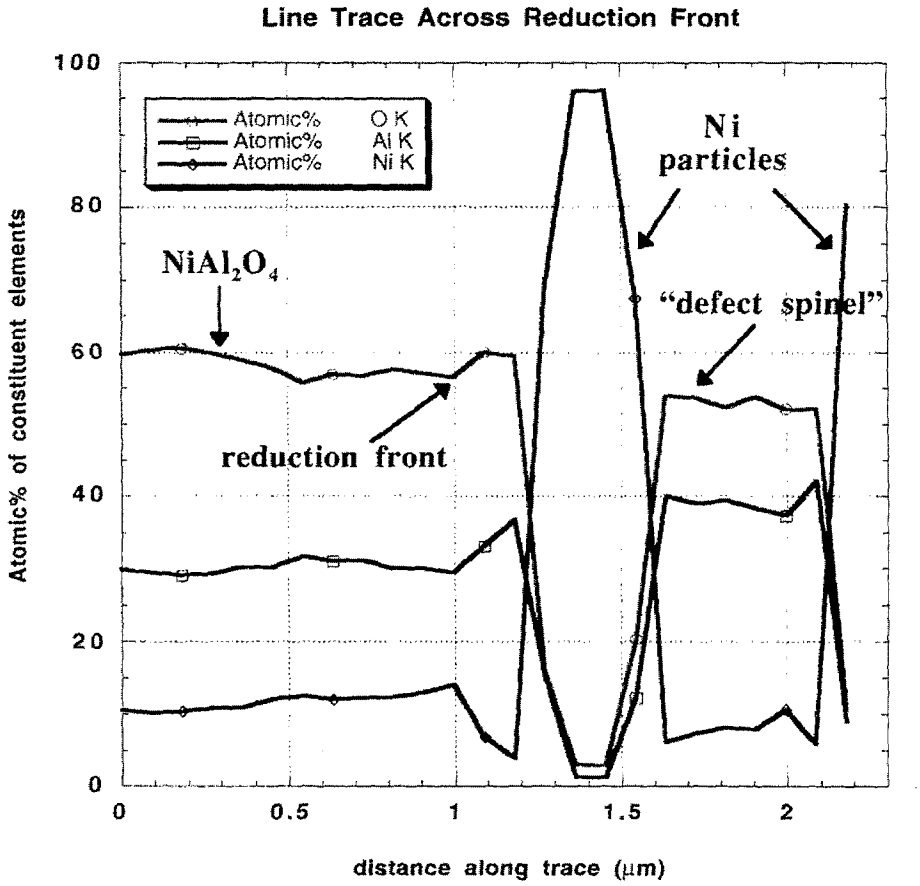


Fig. 5. Chemical composition of phases across the reduction front and along the line in Fig. 4.

variability was less than 1%[1] in bulk density values, less than 10% in total and open porosity and on the order of 20–25% in closed porosity. Thus the density measurements can be considered reproducible (within known experimental errors) for the pellet size employed in this study. The results can be summarized as follows (Table 1 and Fig. 10):

1. Total porosity after reduction varied between 13–24 vol.%. Most of this was open porosity (between 12–23 vol.%, except for # 3 which had about equal amounts of open and closed porosity). Closed porosity was 0.4–3 vol.% and nearly constant in all samples.
2. Final total porosity generally increased with initial total porosity (for a fixed reduction time). However, the difference between the two values actually decreased with sample number or initial total porosity (Fig. 10).
3. There was less variability in average final porosity compared to that in the initial one (Table 1).
4. Longer reduction times led to a denser specimen.

[1] Distinction will be made from this point on between '%' (of a number) and 'vol.%' (e.g. porosity)

Our SEM observations had presented a question about the reason for the apparent decrease in the observed porosity after reduction (Section 3.2). The data in Table 1 clearly proves that the amount of porosity actually increases during reduction leaving only the flaw transformation (in the form of a decrease in the average pore size) as the most probable explanation of the apparent decrease. Our SEM (Fig. 9 (a), where pores about several μm in size are seen) and TEM (Fig. 7) observations support this hypothesis. In Fig. 7, many pores (less than 2 μm) are associated with the large Ni particles located at grain boundaries. These pores are apparently interconnected and have access to the sample surface as can be judged by the large amount of open porosity in Table 1. However, there are also much smaller pores inside the alumina grains (Fig. 11). The small pores are mostly isolated and enclosed by the alumina matrix, i.e. they constitute the closed porosity in Table 1.

Fig. 12 (a) is another bright field image of these small pores. Fig. 12 (b) shows a thickness map of the same region obtained by normalizing the energy-filtered image recorded at the plasmon energy loss of 26 eV by the zero loss image. The pores appear dark in the thickness

map consistent with the fact that these are regions of lower thickness. The image formed using electrons undergoing an energy loss of 8 eV shows uniform intensity suggesting that the pores do not contain any detectable amount of $O_2$. This observation was supported by weight loss data (Section 3.3.3).

*3.3.1.2. Specimens reduced at 1100°C.* The results for samples (all with 2.5 wt.% $ZrO_2$ doping) reduced at 1100°C for 24–36 h in a 10% CO + 90% $N_2$ gas mixture (which is calculated to give an approximate oxygen activity of $10^{-16}$) are presented in Table 2. Note that due to lack of information about the exact value of the theoretical density of 'defect spinel', two different types of closed and total porosity values are shown in this table: The first set is calculated assuming that all the spinel is reduced to Ni and $\alpha$-$Al_2O_3$—similar to the case of 1300°C reductions. The second set is calculated assuming that all of the matrix is $\theta$-$Al_2O_3$ with a crystallographic density of 3.62 g $cm^{-3}$ [14,16,17]. The negative closed porosity values obtained by the latter calculation indicate that the matrix has a higher theoretical density on average than that of $\theta$-$Al_2O_3$ alone. Indeed, it was observed (Fig. 3) that though $\theta$-$Al_2O_3$ was the major phase in the matrix, there were also some additional unidentified peaks which point to the presence of other phases such as $NiAl_{10}O_{16}$. Therefore, the average theoretical density of the matrix is considered to be between that of $\theta$-$Al_2O_3$ and $\alpha$-$Al_2O_3$.


Fig. 6. A typical region from the Ni + 'defect spinel' intermediate layer in the same sample shown in Fig. 4. The dark particles are Ni, the gray regions belong to the matrix and the white areas are pores.

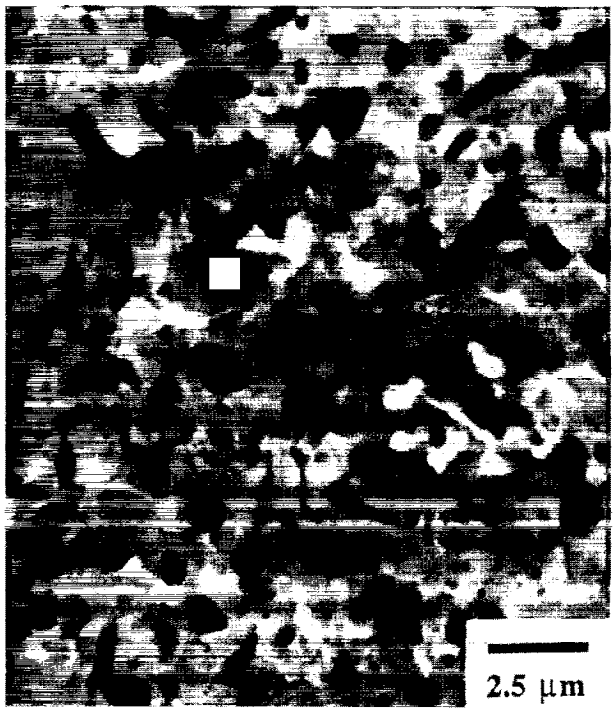


Fig. 7. Equilibrium microstructure in the sample shown in Fig. 4. The dark particles are Ni, the gray is the $\alpha$-$Al_2O_3$ matrix and the porosity is bright.

In sum, the total porosity values after reduction are slightly smaller than those obtained at 1300°C reductions (14–23 vol.%). Again, most of this is open porosity (14–16 vol.%). Examination of Table 2 also shows that upon reduction there is a large increase in the amount of open porosity (about five times) as well as total porosity (about three to four times). Most of the new porosity generated is open.

*3.3.2. Volume change measurements*

Table 1 also exhibits the volume shrinkage data obtained from the same samples reduced at 1300°C used for the density measurements. The volume shrinkage was between 3.2 and 8.8%, with an average value of 5.8%, a value much smaller than the theoretical 17.6%.

Since the volume shrinkage is always below the theoretical value, new open volume inside the sample must be created. In other words, the amount of total porosity should increase after reduction, which is exactly what was observed. In order to see how consistent the porosity and volume change data are and to obtain another independent check of all density and volume change measurements, a simple calculation is proposed: The total amount of porosity in a reduced sample $(P_{total})_{expected}$, should be equal to the initial total porosity $(P_{total})_{initial}$ plus that is generated by the introduction of new, denser phases (i.e. the theoretical volume shrinkage $[\Delta V_{theoretical}]$) minus the amount of volume shrinkage experimentally observed that will decrease the

porosity [$\Delta V_{observed}$]. This calculation is shown in the equation below:

$$(P_{total})_{expected} = (P_{total})_{initial} + \Delta V_{theoretical} - \Delta V_{observed} \quad (2)$$

The results of this calculation as well as the data used are shown in Table 1. For example, for sample # 10, the calculation would be as follows:

$$(P_{total})_{expected} = 8.3 + 91.7 \times 0.173 - 3.3 = 20.9 \text{ vol.\%}$$

where 0.173 is the theoretical volume shrinkage for a sample with 5 wt.% $ZrO_2$.

It is observed that the errors between the calculated and measured total porosity amounts are small (10% or less) and well within the experimental limits. Therefore, this calculation lends validity to the measurements and confirms the fact that the reduced samples are quite porous. Another interesting observation from Table 1 (and Fig. 10) is that the measured volume shrinkage increased with the initial porosity in spinel (for a fixed reduction time).

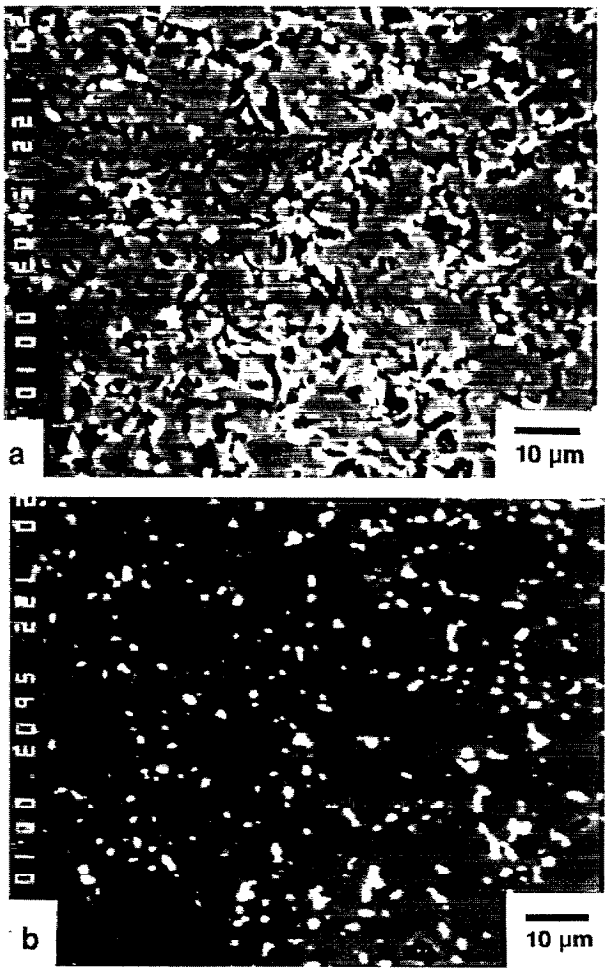


Fig. 8. Scanning electron micrographs which illustrate the effect of mechanical polishing artifacts on the apparent amount of porosity in a spinel specimen. (a) Incorrect polishing procedure described in text. (b) Improved polishing procedure which minimized grain pull-out.

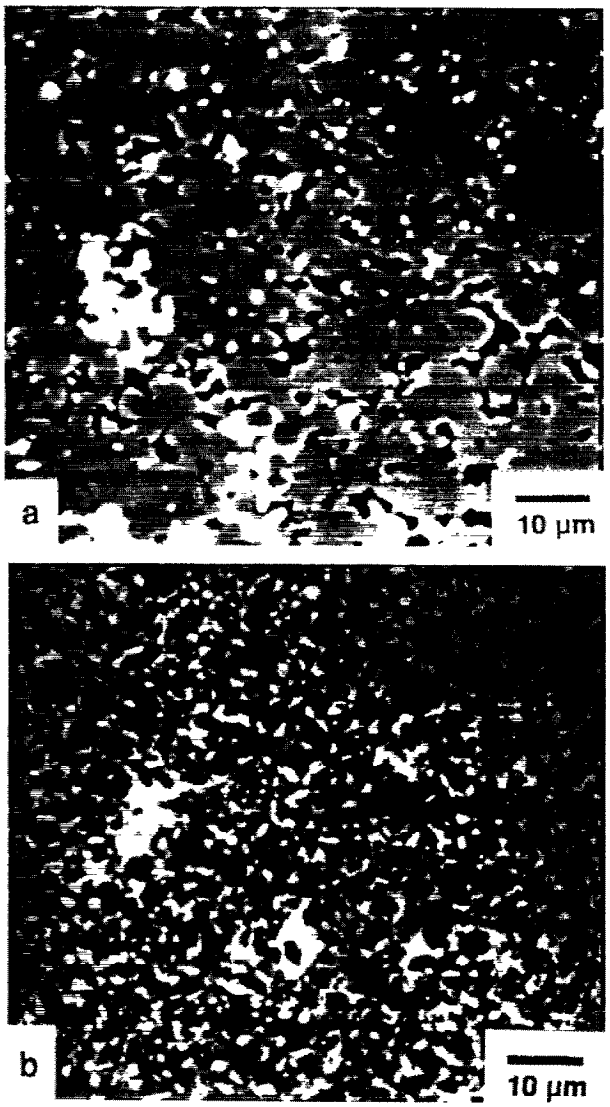


Fig. 9. Scanning electron micrographs of the specimen in Fig. 8: (a) before and (b) after reduction.

The average volume shrinkage measured on five samples reduced at 1100°C for 24–36 h with $a_{O_2} = 10^{-16}$ (10% CO + 90% $N_2$), was 2.1% which is smaller than the average of 5.8% observed from specimens reduced at 1300°C. As mentioned earlier (see Fig. 3), the low temperature reduction leads to the formation of a metastable alumina phase, $\theta$-$Al_2O_3$. The $\theta$-$Al_2O_3$ to $\alpha$-$Al_2O_3$ transformation is calculated to involve a theoretical volume shrinkage of 10.2%. However, the reduction of spinel to $\theta$-$Al_2O_3$ does not involve a large volume shrinkage (as suggested by other researchers) [16,17]. The smaller shrinkage observed at 1100°C and the larger shrinkage measured at 1300°C may be due to the different volume changes associated with formation of $\theta$-$Al_2O_3$ and $\alpha$-$Al_2O_3$.

Table 1
Porosity and volume change data for reduction at 1300°C

| Sample number | Initial total porosity (vol.%) (open, closed) | Volume change ($\Delta V/V_i$) (%) | Predicted final total porosity | Measured final total porosity (vol.%) (open, closed) |
|---|---|---|---|---|
| 1[a] | 1.7 (0.4, 1.3) | −5.0 | 14.0 | 14.4 (14.1, 0.4) |
| 2[a] | 1.9 (0.5, 1.4) | −5.2 | 14.0 | 14.8 (13.7, 1.2) |
| 3[a] | 2.3 (0.8, 1.5) | −7.1 | 12.4 | 12.8 (6.7, 7.1) |
| 4[a] | 3.4 (0.6, 2.8) | −5.6 | 14.9 | 15.6 (14.8, 0.9) |
| 5[a] | 3.5[c] | −8.3 | 12.2 | 13.5 (12.5, 1.2) |
| 6[a] | 4.5[c] | −8.8 | 12.5 | 13.8 (11.6, 2.6) |
| 7[b] | 6.1 (4.0, 2.1) | −3.2 | 19.5 | 20.4 (19.8, 0.5) |
| 8[b] | 6.2 (2.7, 3.5) | −3.8 | 18.6 | 19.3 (18.2, 1.1) |
| 9[b] | 6.4 (4.4, 2.0) | −3.5 | 19.1 | 19.6 (18.5, 1.1) |
| 10[b] | 8.3 (7.1, 1.2) | −3.3 | 20.9 | 19.6 (18.3, 1.3) |
| 11[b] | 8.8 (7.7, 1.1) | −5.1 | 19.8 | 21.7 (20.2, 1.6) |
| 12[b] | 11.2 (11.1, 0.1) | −6.8 | 19.8 | 21.2 (20.2, 1.0) |
| 13[b] | 11.4 (11.2, 0.2) | −6.8 | 19.9 | 21.9 (21.0, 0.9) |
| 14[b] | 12.0 (12.0, 0) | −6.8 | 20.4 | 22.0 (21.1, 0.8) |
| 15[b] | 13.6 (12.9, 0.7) | −7.3 | 21.3 | 24.4 (23.3, 1.1) |
| Average (open, closed) | 6.8 ± 3.8 — | −5.8 (± 1.8) | 17.3 (± 3.3) | 18.3 ± 3.7 (16.9, 1.5) |

[a] Reduced for 24 h; [b] Reduced for 6 h.
[c] Initial porosity was determined by measuring weight and external volume, not by using the ASTM method.

*3.3.3. Weight loss measurements*

The average weight loss obtained in samples reduced at 1300°C for 24 h was 8.8% (± 0.16), while it was 8.5% (± 0.13) for those reduced for 6 h. The low temperature reduction yielded an average weight loss of 8.4% (± 0.07). All of those values are quite close to the theoretical value of 9.1% [10]. The small difference between the theoretical and experimental weight losses may be due to the nonstoichiometry of the initial spinel which was almost always slightly Ni-poor. It is also possible that with longer reductions at high temperature, more oxygen was released to the atmosphere. In any case, however, the reduction nearly reached completion and almost all the oxygen produced in the reaction (Eq. (1)) was released. The STEM observation illustrated in Fig. 12 also supports this conclusion since no oxygen was found inside the small pores.

*3.4. Mechanical properties*

It is well known that the Young's modulus, $E$, of an elastic material is highly sensitive to porosity. The following empirical relation between $E$ at a porosity level $P$ and the fully dense material's modulus, $E_0$, is found to be valid for most ceramics [20]:

$$E = E_0 \cdot (1 - P)^{2n+1} \quad (3)$$

where, $P$ is the volume fraction of porosity and $n$ is the empirical constant ( = 1 for most ceramics).

Fig. 13 plots this equation with $E_0$ calculated to be 340 GPa as the lower Hashin-Shtrikman bound [21] in a 20 vol.% Ni-reinforced $\alpha$-$Al_2O_3$ composite (the Young's moduli for Ni and $\alpha$-$Al_2O_3$ are 200 and 390 GPa, respectively). The lower Hashin-Shtrikman bound was chosen because it is usually a good estimate for the Young's modulus of a metal-reinforced ceramic matrix composite. A reasonably good fit between data and Eq. (3) is obtained in Fig. 13 at low porosity values; however, there is a deviation in the high porosity region. The dotted line shown in Fig. 13 is a fit to the data and is given by:

$$E\ (\mathrm{GPa}) = 376 \cdot (1 - P)^{3.85} \quad (4)$$

The small discrepancy between Eqs. (3) and (4) should be expected, since the validity of the constant $n$ being 1 for metal-ceramic composites is not well established. Nevertheless, however, the Young's moduli of the reduced composites are greatly degraded by the porosity.

*3.5. Generation of stresses due to the volume change*

The preceding sections presented observations of the microstructure evolution during reduction which was presumed to be strongly influenced by the residual stresses generated due to the volume shrinkage. From these results, it can be seen that the system undertakes drastic steps (generation of porosity, formation of metastable phases, etc.) to relax these stresses. A natural question to ask at this point is whether all of these stresses are fully relaxed. Fig. 14 illustrates a model specimen geometry which is currently being investigated to determine the residual stress states of its components. This sample geometry was chosen to explore the possibility of manipulating the unrelaxed residual

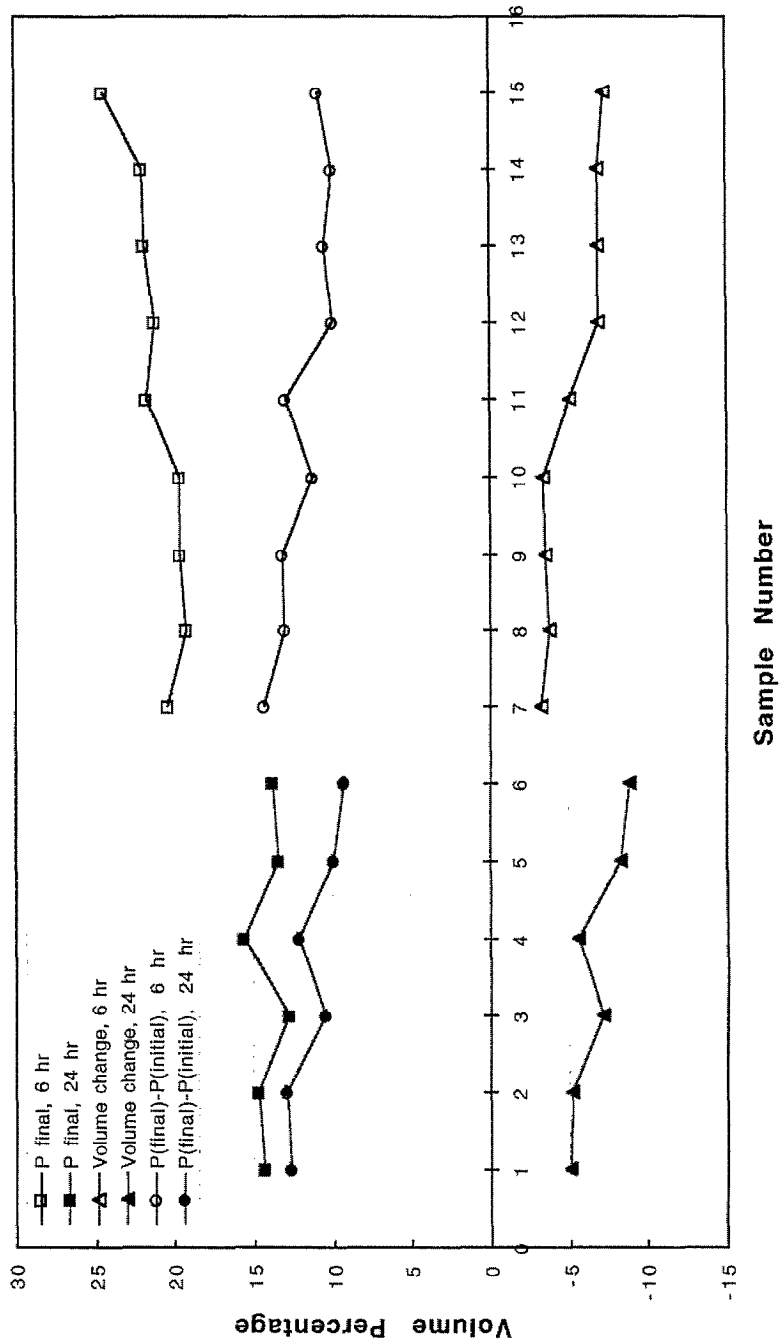


Fig. 10. Plot of porosity and volume change vs. sample number in Table 1.

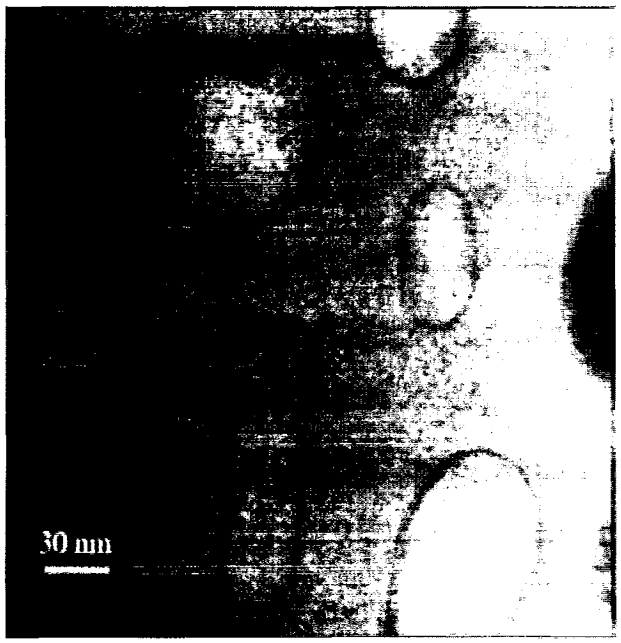


Fig. 11. Bright field scanning transmission electron micrograph of a specimen with 2.5 wt.% $ZrO_2$ and reduced at 1300°C for 4 h at an oxygen activity of $10^{-12}$ showing pores (bright) within an $\alpha$-$Al_2O_3$ grain.

stresses to place a ceramic component in a compressive stress state, i.e. to 'temper' it. Details are given in a future paper; here, only a brief discussion will be presented.

Table 3 summarizes the preliminary stress measurement results and finite element (FE) calculation predictions. The FE calculations assumed elastic deformations and no stress relaxation; therefore, they represent an upper bound for stresses/strains (unpublished). All the stress and strain values shown are in the plane of the middle alumina disk's surface (i.e. along radial or hoop directions) in Fig. 14.

The coefficient of thermal expansion (CTE) mismatch between the two components in this sample (the ring and the alumina disk) will also result in residual stress buildup in the disk. Therefore, a separate FE prediction for such residual stresses is included in Table 3. For specimen A, the Ni + $\alpha$-$Al_2O_3$ reduced composite is estimated to have an average CTE of $9.6 \times 10^{-6}$ $K^{-1}$ (unpublished), whereas for the middle $\alpha$-$Al_2O_3$ disk this value is $8.3 \times 10^{-6}$ $K^{-1}$. In this case, cooling from the reduction temperature will lead to a larger contraction in the composite ring compared to that in the alumina disk resulting in a compressive in-plane residual stress in the latter. On the other hand, for reduction conditions when only the 'defect spinel' is present in the matrix (as in specimen B), the average CTE of the composite is predicted to be smaller than that of $\alpha$-$Al_2O_3$ ($\sim 5.0 \times 10^{-6}$ $K^{-1}$) (unpublished). The CTE mismatch in this case results in a tensile in-plane stress in the alumina disk. Specimen C in Table 3 underwent a different heat treatment procedure: It was first reduced at 1100°C to obtain the Ni + $\theta$-$Al_2O_3$ microstructure. It was then held at 1250°C to transform some of the $\theta$-$Al_2O_3$ in the matrix to $\alpha$-$Al_2O_3$. XRD measurements showed that 35% of the matrix is still $\theta$-$Al_2O_3$ [7]. The CTE of the reduced composite in this specimen was calculated to be the volume-weighed average of those in the other two specimens ($\sim 8.0 \times 10^{-6}$ K) [7]. A further complication in all these predictions

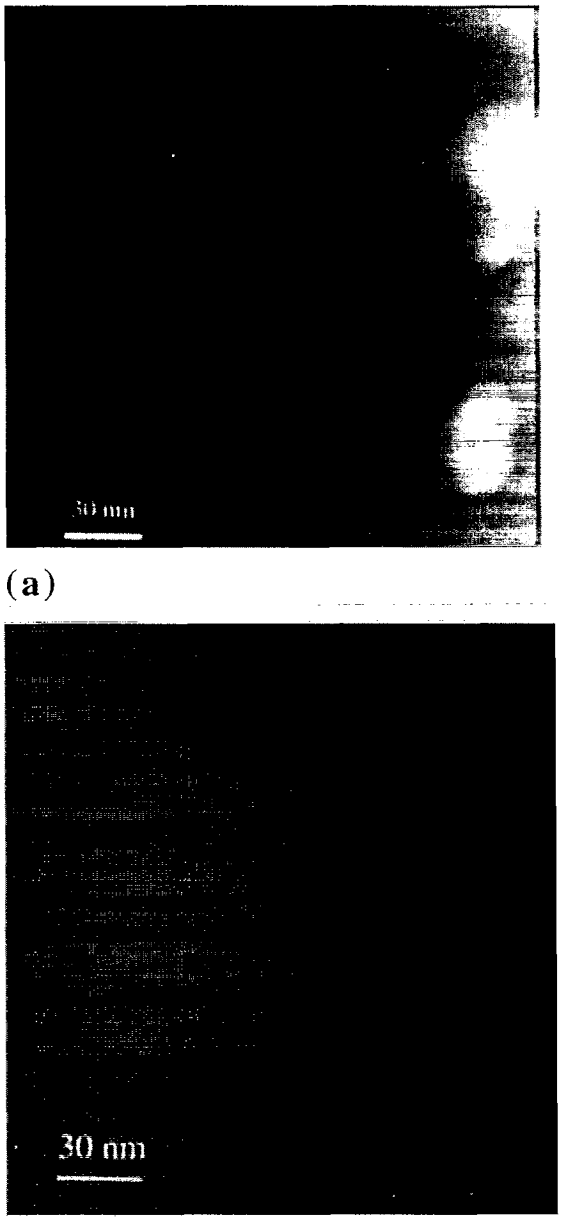


Fig. 12. (a) Bright field and (b) normalized plasmon loss energy-filtered images of a region from the same sample shown in Fig. 11 recorded in the STEM. The voids appear dark in the plasmon loss image, which is a thickness map with the thicker regions appearing bright.

Table 2
Porosity data for reduction at 1100°C

| Sample number | Open porosity (vol.%) | | Closed porosity (vol.%) | | Total porosity (vol.%) | |
|---|---|---|---|---|---|---|
| | Unreduced | Reduced | Unreduced | Reduced | Unreduced | Reduced |
| 91 | 1.6 | 13.8 | 2.5 | 6.1[a]<br>−0.3[b] | 4.1 | 19.9[a]<br>−13.5[b] |
| 92 | 3.0 | 16.8 | 3.8 | 6.1[a]<br>−0.1[b] | 6.7 | 22.8[a]<br>16.7[b] |
| 93 | 2.5 | 15.2 | 2.5 | 5.0[a]<br>−1.4[b] | 5.0 | 20.1[a]<br>13.8[b] |
| 94 | 4.7 | 15.8 | 1.8 | 5.0[a]<br>−1.3[b] | 6.5 | 20.8[a]<br>14.5[b] |
| 95 | 4.2 | 16.2 | 1.0 | 4.4[a]<br>−1.8[b] | 5.2 | 20.7[a]<br>14.4[b] |
| Average | 3.2 ± 1.1 | 15.6 ± 1.0 | 2.3 ± 0.9 | 5.3 ± 0.7[a]<br>−0.98[b] (± 0.66) | 5.5 ± 1.0 | 20.9[a] (± 1.0)<br>14.6[b] (± 1.1) |

[a] Calculated assuming matrix is 80 vol.% $\alpha$-$Al_2O_3$.
[b] Calculated assuming matrix is 80 vol.% $\theta$-$Al_2O_3$.

is the effect of porosity on the CTE of the reduced composite. Work is in progress to investigate this issue as well as to experimentally determine all CTE values using dilatometry.

The preliminary X-ray and neutron diffraction data in Table 3 suggest that the majority of the residual stresses due to the volume change is relaxed. None of the specimens exhibited a large compressive in-plane stress in the alumina disk. The observation of a small tensile stress in specimen C clearly indicates that the volume change was not as effective and that most of the stresses due to that effect are relaxed. However, specimen B shows a small compressive stress in the alumina disk which, when compared to FE predictions, suggests that the volume change due to reduction is counteracting the CTE-mismatch effect. Work is in progress to confirm the above data and correlate it with FE predictions [7]. At this stage, our principal conclusion is that, for the reduction conditions applied to samples mentioned here, most of the volume-change-induced residual stresses appear to be relaxed at the reduction temperature.

## 4. Discussion

The XRD and neutron results clearly showed that the stresses predicted by FE alone were not present in the test specimens. However since the FE calculations only describe the elastic deformations and assume certain values for CTE and shrinkage, they do not incorporate any microstructrural relaxation effects.

The premise for using a partial reduction to 'temper' a ceramic relies on the volume shrinkage associated with the reaction. Assuming a compacted spinel cylinder in which the reaction proceeds from the surface, the volume shrinkage (for $NiAl_2O_4$ it is theoretically 17.6%) will compress the interior. In the absence of any relaxation mechanisms, if the reduction is stopped prior to completion when the reduced composite surrounds an unreduced spinel core, the reduced region will experience a hoop tensile strain, whereas the interior will experience an approximately hydrostatic compressive strain. The associated residual stresses can rapidly approach GPa in simple geometries. However the potential for developing these residual stresses depends on the ability of the material to avoid stress buildup by creep, plastic deformation or cracking. Accordingly the coupling between residual stress and microstructure development is subtle and complicated.

One complicating feature in predicting the shrinkage and stress development is that the reduction can undergo an intermediate state prior to completion. For reductions performed at low temperatures (1100°C) the reduction products include metastable phases that evolve prior to the formation of the equilibrium $\alpha$-$Al_2O_3$ matrix. These are called 'defect spinel' and consist of Ni-poor phases with complex crystal structures. Some (e.g. $NiAl_{10}O_{16}$) have a large number of twin variants that can reduce the strain energy [18]. The major phase in 'defect spinel' appears to be the metastable monoclinic (nearly cubic) $\theta$-$Al_2O_3$. This phase is often obtained when a cubic oxygen sublattice (for example, in $\gamma$-$Al_2O_3$ which has a spinel structure) is transformed into a hexagonal one (in $\alpha$-$Al_2O_3$) [14,16,17]. The significance of this intermediate reduction stage is that there is little volume change associated with the formation of $\theta$-$Al_2O_3$; whereas the $\theta$ to $\alpha$-transformation involves the desired shrinkage [16,17]. Accordingly, the reduction reaction can be more accurately represented by:

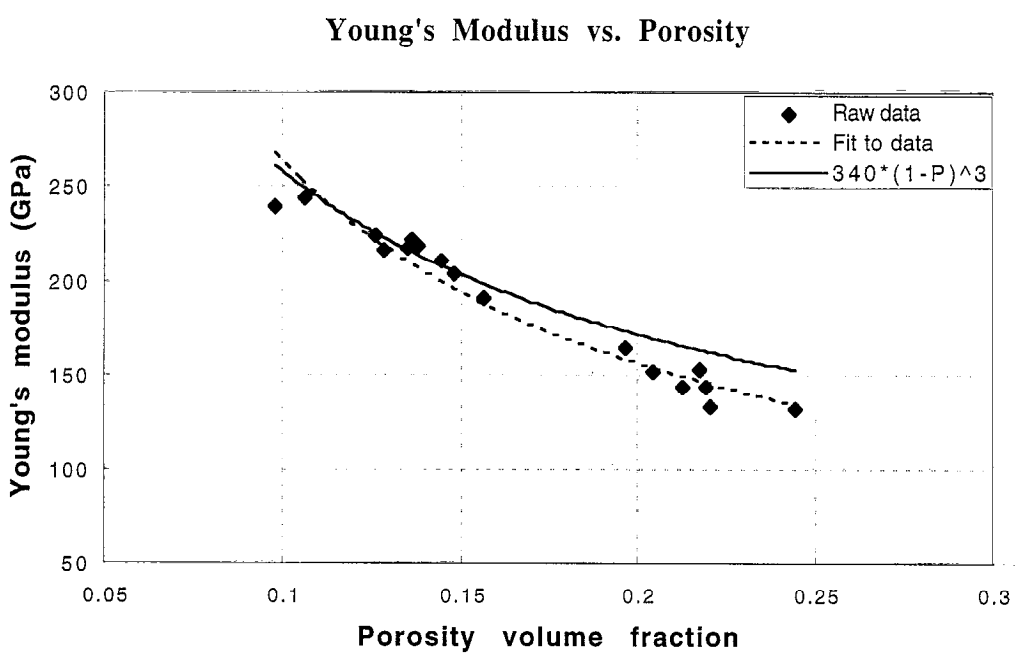


Fig. 13. Comparison of experimentally determined Young's moduli of Ni-alumina composites obtained by reduction at 1300°C to Eq. (3) with $n = 1$ (solid line).

$$NiAl_2O_4 \Rightarrow Ni + \text{'defect spinel'}\ (\theta\text{-}Al_2O_3) \Rightarrow Ni + \alpha\text{-}Al_2O_3 \quad (5)$$

At the intermediate step Ni is precipitated to form almost pure metallic Ni particles while TEM suggests that the matrix undergoes complex twinning, presumably to relieve stress buildup.

Another microstructural variable implicit in the reduction that should be considered in the context of stress development is porosity. During the reduction of the outer region the interior unreduced portion effectively experiences an in situ hot isostatic pressing. The pressure may collapse the porosity present in spinel and lead to densification as supported by a comparison of Figs. 7 and 9. Pores of diameter 5–10 μm prior to reduction (Fig. 9) are replaced by smaller ones with diameters less than 2 μm (Fig. 7) at alumina grain boundaries and even smaller ones with diameters of 20–250 nm inside alumina grains (Fig. 11). Since the volume shrinkage is larger for specimens with a larger starting porosity (Fig. 10 and Table 1) this suggests that it is easier to compress (and densify) a porous sample. A supporting evidence is the fact that the difference between final and initial porosity decreases with the initial porosity increase (Fig. 10). However, we have insufficient data at this time to infer the impact on stress development.

Another feature linked to the porosity is that a porous sample can be reduced faster. Since sintering is expected to follow the reduction (provided that the sample is held long enough at the reduction temperature), a porous specimen will have more time to sinter than its dense counterpart, assuming that both are fully reduced. It is likely that sintering is occurring in our specimens. Samples with similar initial porosity values (e.g. #6 and 7 in Table 1) show markedly different final porosities due to the difference in reduction times. Moreover, doping with $TiO_2$ (which acts as a sintering agent for alumina) drastically increased the shrinkage and reduced the final porosity for a given time [5]. One experiment that can determine whether in situ hot isostatic pressing occurs is in situ neutron diffraction that can monitor phase and strain evolution during reduction. We are currently engaged in a study to perform such an experiment using a controlled atmosphere furnace [22].

It must also be noted that the density measurements clearly show that the total amount of porosity actually increases during reduction. So the simple concept that the volume change due to reduction generates large stresses which can heal flaws is not correct. Instead, a more complex behavior is seen, where large-diameter pores are removed and replaced by a much larger volume fraction of small-diameter pores. This can be thought of as flaw transformation, not flaw healing. More work is needed to obtain quantitative data about the change in the average size of pores during reduction.

Unfortunately a calculation that predicts the densification of the unreduced spinel together with porosity growth in the reduced layer driven by the reaction self-stress due to the volume change is not currently possible due to lack of data concerning either the high temperature mechanical properties (creep and plastic

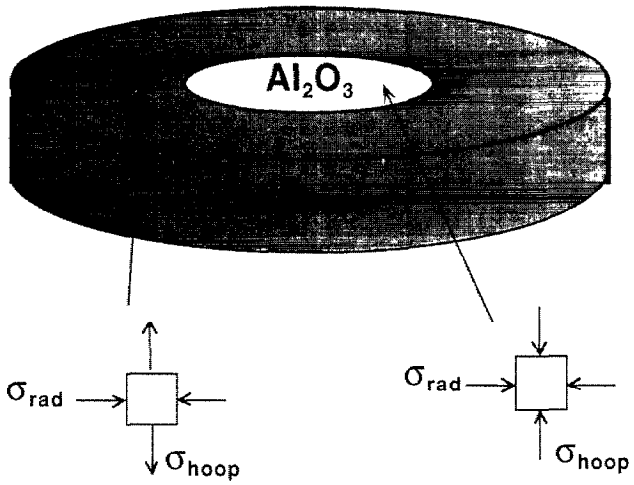


Fig. 14. Model specimen which illustrates how a volume decrease in the outer spinel ring can generate compressive stresses in the inner $\alpha$-$Al_2O_3$ disk. Actual specimens have an overall diameter of 10 mm and thickness $\approx 2$–5 mm. The middle alumina cylinder has 4 mm diameter. The predicted in-plane stress state after reduction in each component is also shown.

deformation) or the diffusivities of the various species that determine the reaction rate.

The overall result of all the possible stress relaxation mechanisms mentioned above appears to be that the majority of the volume-change-induced residual stresses are relieved during reduction for certain reduction conditions. However, it may be possible to develop processing routes to reduce stress relaxation as was shown for specimen B in Table 3. Our goal is then to manipulate these residual stresses to 'temper' ceramics for improved fracture resistance.

## 5. Conclusions

(1) The reduction of $NiAl_2O_4$ to Ni + '$Al_2O_3$' involves a volume shrinkage that can generate residual stresses.

(2) An intermediate step is observed during partial reduction where metastable phases form, presumably to relax the residual stresses.

(3) There is an increase in the amount of porosity present in specimens after reduction, leading to a smaller observed volume change, likely to minimize the build-up of residual stresses.

Table 3
Summary of residual stress measurements

| Method | Specimen A Reduced at 1300°C | Specimen B Reduced at 1100°C | Specimen C Reduced at 1100°C; heat treated at 1250°C |
|---|---|---|---|
| Finite Element Prediction (on the surface of the center of alumina disk) | $\sigma \approx -100$ MPa (CTE)[a]<br>$\sigma \approx -1200$ MPa ($\Delta V$+CTE)[b] | $\sigma \approx +280$ MPa (CTE)[a]<br>$\sigma \approx -270$ MPa ($\Delta V$+CTE)[b] | $\sigma \approx +125$ MPa (CTE)[a]<br>$\sigma \approx -660$ MPa ($\Delta V$+CTE)[b] |
| X-ray Diffraction (on the surface of the center of alumina disk) | $\sigma \approx -130$ MPa ($\pm 50$) | $\sigma \approx -72$ MPa ($\pm 50$) | $\sigma \approx +25$ MPa ($\pm 50$) |
| Neutron Diffraction (volume average of alumina disk) | $\sigma \approx -103$ MPa[c,d] ($\pm 40$) | $\sigma \approx +37$ MPa ($\pm 40$)[d] | — |

[a] Due to the CTE mismatch between the reduced composite ring and the alumina disk (Fig. 14)
[b] Due to the combined effects of volume shrinkage during reduction and the CTE mismatch between the two regions in Fig. 14.
[c] This value should be viewed with caution since there were two $\alpha$-$Al_2O_3$ phases under different stress states: One in the disk; the other in the reduced ring. The whole sample contributed to the same diffraction pattern; therefore, no discrimination between the two phases was possible. A new measurement will be performed with a collimated neutron beam to distinguish between these phases.
[d] Stresses were calculated from the Hooke's law for isotropic elasticity using the experimentally determined strains.

(4) Flaw healing in the form of a decrease in porosity by the in situ hot isostatic pressing of the unreduced portion of spinel does not occur, since there is an increase in total porosity after reduction. The average pore size appears to decrease during reduction pointing to the possibility of flaw transformation. In situ neutron diffraction experiments to monitor phase and residual stress evolution during reduction should clarify whether or not in situ hot isostatic pressing occurs.

(5) The majority of the residual stresses due to the volume shrinkage during partial reduction are relaxed. There are other processing routes which yield less relaxation and allow the generation of residual stresses that can be used to 'temper' ceramics.

## Acknowledgements

This work was supported by the US Office of Naval Research under Grant No. N00014-92-J-1526 at Cornell University and by a Laboratory Directed Research and Development project at Los Alamos National Laboratory. E. Üstündag acknowledges the financial support by a Director-Funded Post-doctoral Fellowship at Los Alamos. S. Subramanian was supported by the US Department of Energy Grant No. DE-FG02-85ER45211 at Cornell. ML Stocker began this study as a project for an undergraduate Materials Science and Engineering Research Involvement course. The Manuel Lujan Jr. Neutron Scattering Center at Los Alamos is a national user facility supported by DOE/DP and DOE/BES under contract W-7405-ENG-36. The use of the Materials Preparation, X-ray and Electron Microscopy facilities of the Materials Science Center at Cornell University, which is supported by the National Science Foundation is also acknowledged.

## References

[1] E. Üstündag, R. Subramanian, R. Dieckmann, S.L. Sass, Acta Metall. Mater. 43 (1995) 383.
[2] F.A. Elrefaie, W.W. Smeltzer, J. Electrochem. Soc. 128 (1981) 2237.
[3] E. Üstündag, Processing, structure and characterization of in-situ-formed metal-ceramic composites obtained by partial reduction reactions, PhD Thesis, Cornell University, USA, 1995, p. 158.
[4] E. Üstündag, P. Ret, R. Subramanian, R. Dieckmann, S.L. Sass, Mater. Sci. Eng. A195 (1995) 39.
[5] Z. Zhang, In situ nickel-alumina composites obtained by partial reduction of nickel aluminate spinel: Processing, microstructure, characterization and the influence of doping, PhD Thesis, Cornell University, 1997, USA.
[6] E. Üstündag, M.L. Stocker, Y. Shapiro, J.E. Trancik, S.L. Sass, in: T.S. Srinivasan, J.J. Moore (Eds.), Processing and Fabrication of Advanced Materials IV, The Minerals, Metals and Materials Society (TMS), Warrendale, PA, 1996, pp. 529.
[7] C.C. Ahn, O.L. Krivanek, EELS Atlas, Gatan, 1983.
[8] R.F. Egerton, Electron Energy-Loss Spectroscopy in the Electron Microscope, 2nd edn., Plenum Press, New York, 1996.
[9] ASTM Standard C 373-88, American Society for Testing and Materials, Philadelphia, PA, 1988.
[10] E. Üstündag, Processing, structure and characterization of in-situ-formed metal-ceramic composites obtained by partial reduction reactions, PhD Thesis, Cornell University, 1995, pp. 84–96.
[11] D.J. Babikov, Ulrasonics and Its Industrial Applications, Consultants Bureau, New York, 1960.
[12] I.C. Noyan, J.B. Cohen, Residual Stress, Springer-Verlag, New York, 1987, pp. 117–130.
[13] M.T. Hutchings, A.D. Krawitz (Eds.), Measurement of Residual and Applied Stress Using Neutron Diffraction, NATO ASI Series 216E, Kluwer, Dordrecht, 1992, pp. 93–112.
[14] S.J. Wilson, J.D.C. McConnell, J. Solid State Chem. 34 (1980) 315.
[15] E. Üstündag, Processing, structure and characterization of in-situ-formed metal-ceramic composites obtained by partial reduction reactions, PhD Thesis, Cornell University, 1995, pp. 131–144.
[16] S.J. Wilson, Proc. Br. Ceram. Soc. 28 (1979) 281.
[17] S.J. Wilson, M.H. Stacey, J. Colloid Interface Sci. 82 (1981) 507.
[18] P. Bassoul, J.C. Gilles, J. Solid State Chem. 58 (1985) 383.
[19] Z. Zhang, E. Üstündag, S.L. Sass, in: J.S. Im, B. Park, A.L. Greer, G.B. Stephenson (Eds.), Thermodynamics and Kinetics of Phase Transformations, Proceedings of the MRS, vol. 398, Materials Research Society, Pittsburgh, PA, 1996, p. 489.
[20] K.K. Phani, S.K. Miyogi, J. Mater. Sci. 5 (1986) 427.
[21] Z. Hashin, S. Shtrikman, J. Mech. Phys. Solids 11 (1963) 127.
[22] E. Üstündag, M.A.M. Bourke, Experiment report, 1996, Manuel Lujan Jr. Neutron Scattering Center, Los Alamos National Laboratory, Los Alamos, NM.